The Role of Serine Coordination in the Structural and Functional Protection of the Nitrogenase P-cluster

Hannah L. Rutledge,[1] Mackenzie J. Field,[2] Jonathan Rittle,[1, †] Michael T. Green,[2,3] F. Akif Tezcan*[,1]

[1] Department of Chemistry and Biochemistry, University of California, San Diego, 9500 Gilman Drive, La Jolla, California 92093-0356, United States.

[2] Department of Chemistry, University of California, Irvine, Irvine, California 92697, United States.

[3] Department of Molecular Biology and Biochemistry, University of California, Irvine, Irvine, California 92697, United States.

* tezcan@ucsd.edu

ABSTRACT: Nitrogenase catalyzes the multi-electron reduction of dinitrogen to ammonia. Electron transfer in the catalytic protein (MoFeP) proceeds through a unique [8Fe-7S] cluster (P-cluster) to the active site (FeMoco). In the reduced, all-ferrous (P^N) state, the P-cluster is coordinated by six cysteine residues. Upon two-electron oxidation to the P^{2+} state, the P-cluster undergoes conformational changes in which a highly conserved oxygen-based residue (a Ser or a Tyr) and a backbone amide additionally ligate the cluster. Previous studies of *Azotobacter vinelandii* (*Av*) MoFeP revealed that when the oxygen-based residue, βSer188, was mutated to a non-ligating residue, Ala, the P-cluster became redox-labile and reversibly lost two of its eight Fe centers. Surprisingly, the *Av* strain with a MoFeP variant that lacked the serine ligand (*Av* βSer188Ala MoFeP) could still grow and fix nitrogen as quickly as wild-type *Av* MoFeP, calling into question the necessity of this conserved ligand for nitrogenase function. Based on these observations, we hypothesized that βSer188 plays a role in protecting the P-cluster under non-ideal conditions. Here, we investigated the protective role of βSer188 both *in vivo* and *in vitro* by characterizing the ability of *Av* βSer188Ala cells to grow under suboptimal conditions (high oxidative stress or Fe limitation) and by characterizing the ability of *Av* βSer188Ala MoFeP to be mismetallated *in vitro*. Our results demonstrate that βSer188 (1) increases *Av* cell survival upon exposure to oxidative stress in the form of hydrogen peroxide, (2) is necessary for efficient *Av* diazotrophic growth under Fe-limiting conditions, and (3) protects the P-cluster from metal exchange *in vitro*. Taken together, our findings suggest a structural adaptation of nitrogenase to protect the P-cluster via Ser ligation, which is a previously unidentified functional role of the Ser residue in redox proteins and adds to the expanding functional roles of non-Cys ligands to FeS clusters.

Introduction

Nitrogenase is the only known enzyme capable of catalyzing the reduction of atmospheric dinitrogen (N_2) into ammonia (NH_3) (Equation 1).[1-4]

$$N_2 + 8e^- + 8H^+ + n\text{ATP} \rightarrow 2NH_3 + H_2 + n\text{ADP} + nP_i \quad (1)$$

The most widely studied version of nitrogenase is the Mo-nitrogenase which comprises two component proteins: the iron-protein (FeP), which serves as the reductase/ATPase, and the molybdenum-iron protein (MoFeP) which performs N_2 reduction.[5] The multi-electron reduction of N_2 to NH_3 is both thermodynamically and kinetically challenging,[6] requiring precise coordination of electron and proton transfer events within the nitrogenase complex to preferentially reduce N_2 over protons (H^+).[2] Electron transfer (ET) to the active site begins at the [4Fe-4S] cluster in FeP, proceeds through the intermediary [8Fe-7S] P-cluster in MoFeP, and ends at the site of catalysis, the iron-molybdenum-cofactor (FeMoco).[1] Many successive cycles of one- (or possibly two-)[7-9] ET steps are required for the reduction of a single N_2 molecule, with each turnover cycle requiring ATP-gated association and dissociation of the FeP-MoFeP complex.

The distinct structure and composition of FeMoco are ultimately responsible for this cofactor's ability to efficiently reduce N_2. Yet, nitrogenase is also unique in its use of an expanded (i.e., the P-cluster)[10-11] rather than a canonical Fe-S cluster (i.e., [2Fe-2S], [3Fe-4S], [4Fe-4S])[12-14] as an electron relay center, implying that the P-cluster may not merely act as a passive one-electron transfer conduit. Aside from its composition, the P-cluster is also

distinct in terms of its coordinating ligands (Figure 1a).[15] In canonical Fe-S clusters, every Fe atom is coordinated to a terminal side-chain ligand from the protein.[14] In contrast, the P-cluster is coordinated by both bridging and terminal cysteine (Cys) residues, which enables the cluster to undergo substantial structural changes in an oxidation-state-dependent manner.[15] In the dithionite (DT)-reduced, all-ferrous state (P^N), the P-cluster is coordinated by six Cys (four terminal and two bridging) residues (Figure 1a, 1c top).[15] Upon oxidation by one electron to reach the P^{1+} state, a serine (Ser) residue (βS188 in *Azotobacter vinelandii* (*Av*) MoFeP) ligates an Fe center (Fe6), resulting in the opening of one cubane half of the cluster proximal to the β-subunit of MoFeP.[16-17] Oxidation by one more electron to reach the P^{2+} state (also termed P^{OX}) is accompanied by the coordination of another Fe center (Fe5) by the backbone amidate N of a bridging Cys (αC88) (Figure 1c).[15-16] Interestingly, βS188 is not strictly conserved: many nitrogenases contain an alanine (Ala) in position β188 (*Av* numbering).[18] Yet, all but one of such nitrogenases contain a tyrosine (Tyr) in an alternative position (β99, *Av* numbering), which acts similarly to βS188 as a redox-switchable ligand, as recently demonstrated in the case of MoFeP from *Gluconacetobacter diazotrophicus* (*Gd*).[18] The strict conservation of a covariant Ser or Tyr residue as a P-cluster ligand across all known nitrogenase sequences (with only one exception; see Conclusions) strongly suggests that presence of a hard, O-based ligand is important for nitrogenase function.[18] It has been proposed that the binding of FeP to MoFeP during catalysis might trigger the coordination of the Ser or Tyr ligand to the P-cluster, thereby decreasing the reduction potential of the cluster and triggering ET from the P-cluster to FeMoco.[1, 18-20] Alternatively, FeP-MoFeP complexation may induce conformational changes near FeMoco to increase its reduction potential and drive gated ET from the P-cluster. In this scenario, which is supported by recent cryoEM structures of the FeP-MoFeP complex isolated during catalytic turnover,[21] Ser- or Tyr-ligation would serve to stabilize the resulting oxidized P-cluster, thus serving as a redox ratchet (rather than a trigger).

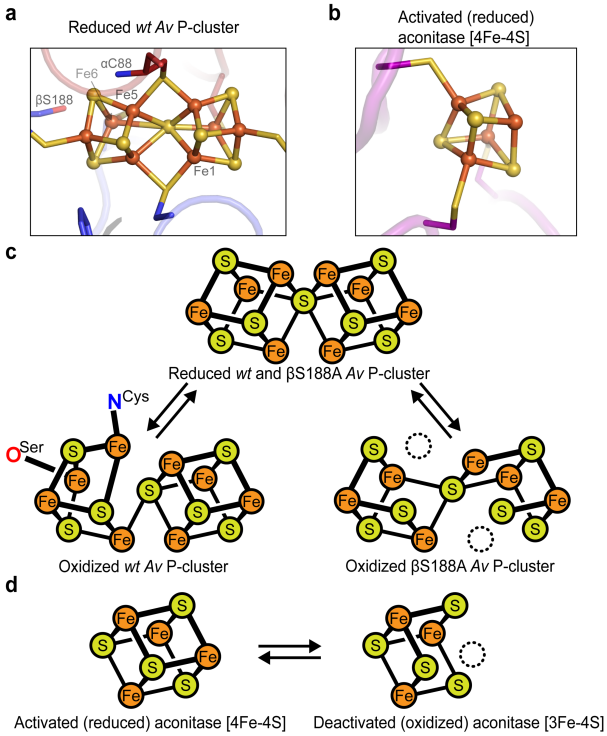

Figure 1. Examples of coordinatively unsaturated Fe-S clusters including the nitrogenase P-cluster and the [4Fe-4S] active site of aconitase. (a) The fully-reduced *Av* nitrogenase P-cluster (P^N) is coordinated by four terminal and two bridging Cys residues. (PDB ID: 3MIN) (b) Activated aconitase contains a coordinatively unsaturated [4Fe-4S] cluster. The non-Cys-ligated Fe is coordinated to a water molecule (not shown). (PDB ID: 6ACN) (c) Two-electron oxidation of the *Av* MoFeP P-cluster results in coordination by βS188 and the backbone amide of αC88. The βS188A *Av* MoFeP mutant contains two redox-labile Fe centers (dashed circles, Fe1 and Fe5). (d) The [4Fe-4S] cluster in aconitase contains one redox-labile Fe center (dashed circle).

Ser- or Tyr-coordinated Fe-S clusters are very rare, and the few established cases are not involved in electron relay.[22-24] To elucidate the functional role of these oxygenic ligands to the P-cluster, we previously characterized a *Av* MoFeP mutant that lacked βS188 (βS188A MoFeP) and found that this residue was required to maintain the redox-dependent structural integrity of the P-cluster.[19] Notably, the oxidation of βS188A MoFeP led to the labilization and loss of two of the Fe centers (Fe1 and Fe5) of the P-cluster, yielding a cluster composed of two [3Fe-4S] units that shared a bridging sulfide (Figure 1c).[19] Surprisingly, we also observed that the redox-instability of the P-cluster did not affect the diazotrophic growth rate of the βS188A *Av* strain, and the βS188A MoFeP mutant was as catalytically active as wild-type (*wt*) MoFeP for N_2 reduction *in vitro*.[19] These results called into question whether the Ser (or Tyr) ligand to the P-cluster was actually required for nitrogenase catalysis in *Av*.

The redox-labile βS188A P-cluster is reminiscent of some biological [4Fe-4S] clusters that can lose an Fe to form [3Fe-4S] clusters (Figure 1b,d). Such labile Fe-S clusters are found in some ferredoxins (including *Pyrococcus furiosus* Fd, *Desulfovibrio vulgaris* Fd I, and *Desulfovibrio africanus* Fd III)[25] and in a family of enzymes that use the cluster as a catalytic Lewis acid site (e.g., dihydroxy-acid dehydratase,[26] fumarases A and B,[27] and aconitases[28-29]). In all of these clusters, only three of the Fe centers are Cys-ligated. In the case of the ferredoxins, the fourth Fe is either coordinated by a non-Cys residue (e.g., Asp),[25] or, in the case of Lewis acidic active sites, by an aqua ligand.[30] Analogous to the βS188A P-cluster, these dynamic clusters are prone to oxidative damage: upon oxidation to $[4Fe\text{-}4S]^{3+}$, the non-Cys-ligated Fe dissociates from the cluster, leading to its inactivation (Figure 1d).[25, 27, 31-35]

In addition to their sensitivity to oxidation, some of these clusters also suffer from demetallation when the cellular labile Fe pool (LIP) is low in concentration[36] and from mismetallation when they are reconstituted in the presence of other metal ions.[25, 37-42]

Based on the similarities between the βS188A P-cluster and the redox-labile [4Fe-4S] clusters in other redox proteins, we hypothesized that (1) the *Av* βS188 P-cluster ligand may serve to protect the P-cluster from oxidative damage and mismetallation, and (2) this role may not have been evident under the ideal, Fe-replete conditions previously used to measure βS188A *Av*'s diazotrophic growth rate and *in vitro* catalytic activity.[19] To investigate this hypothesis, we probed in this study whether βS188A *Av* cells were more prone to oxidative stress than *wt* cells and measured the growth rate and *in vivo* activity of *Av* βS188A under non-ideal, Fe-limited conditions. Additionally, we examined the capacity of the βS188A P-cluster to be heterometallated *in vitro* by crystallographic, spectroscopic, and analytical methods. Our results provide strong evidence for the previously unconsidered role of the Ser ligand in protecting the structural and functional integrity of the P-cluster under environmental duress. They also show that the P-cluster is inherently more dynamic than originally envisioned, capable of undergoing extensive metal exchange reactions upon oxidation.

Results and Discussion

In vivo effects of the βS188A mutation

We initially investigated what, if any, protective roles the Ser ligand to the P-cluster may provide *in vivo*. To this end, we carried out an oxidative stress test of *Av* βS188A cells in which we measured cell survival after 30 minutes of exposure to 5 mM hydrogen peroxide (H_2O_2) using previously reported procedures, which had used 15 mM H_2O_2 (Figure 2a).[43-44] Increasing catalase activity, which catalyzes the decomposition of H_2O_2 into H_2O and O_2, has been

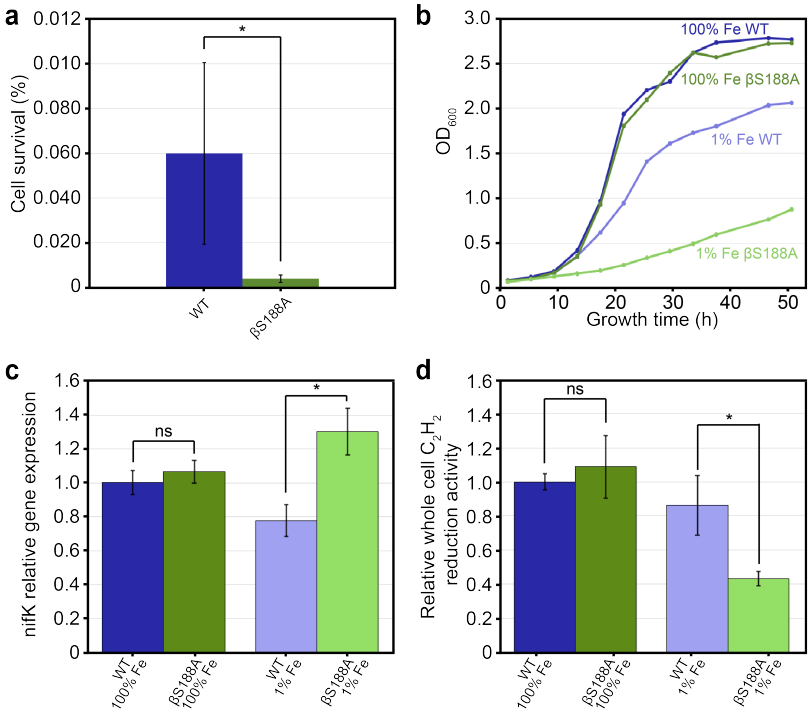

Figure 2. ***In vivo* experiments to examine the physiological role of βS188 ligand to the P-cluster in *Av* MoFeP.** The color scheme for the variants is as follows: *wt* (dark and light green) and βS188A MoFeP (dark and light blue). Error bars represent one standard deviation of experiments performed at least in triplicate. Statistical significance is represented by "ns" (not significant) or * (p-value < 0.05). (a) Oxidative stress test of *Av* cells represented as percent cell survival determined via colony forming units (CFUs) before and after 30 min exposure to 5 mM H_2O_2. Cells were grown diazotrophically with 35 μM Fe (100% Fe). The experiment was performed in biological triplicate. (b) Growth curves of *Av* wt and *Av* βS188A cells in cultures with 100% and 1% Fe (0.4 μM). (c) RT-qPCR of *nifK* gene expression of *wt* and βS188A *Av* grown diazotrophically with varying amounts of Fe. Expression levels were normalized to the expression level of reference gene *rho*, and the data is presented relative to *wt Av* cells grown diazotrophically with 100% Fe. The experiment was carried out in technical triplicate of biological triplicates. (d) *Av* cell cultures used for RT-qPCR in (c) were also used for whole cell C_2H_2 reduction assays (biological triplicate). C_2H_4 produced was measured and normalized to both the relative *nifK* transcript levels and the OD_{600} of the cells, then presented relative to *wt Av* grown with 100% Fe.

shown to augment the cellular efficiency of nitrogenase in the diazotroph *Rhizobium leguminosarum*, indicating that oxidative stress and nitrogenase activity are intertwined.[45] If the Ser ligand is protective of the *wt* P-cluster during *in vivo* catalysis, we hypothesized that βS188A MoFeP would be more prone to oxidative stress and release Fe from the P-cluster when grown diazotrophically, thereby resulting in lower survival rates than *wt* MoFeP. Indeed, we found that the survival frequency of the H_2O_2-treated βS188A *Av* cells was only 7% of that of *wt Av* cells, indicating that the mutant cells were significantly more prone to oxidative stress when grown diazotrophically.

When culturing *Av* cells, the medium is typically supplemented with Fe to allow for rapid cell growth.[46] The Burke's medium used in our protocols contains 35 μM Fe, hereafter referred to as 100% Fe. If the Fe centers of the βS188A MoFeP P-cluster are labilized during catalysis under physiological conditions, the high Fe concentration in the 100% Fe medium may be beneficial either by maintaining a large cellular LIP (which in turn could enable fast reconstitution of the labile P-cluster during *in vivo* catalysis) or by providing excess Fe to enable higher levels of MoFeP expression. To probe these possibilities, we investigated the diazotrophic growth rates of *wt* and βS188A *Av* cells in media with varying concentrations of Fe (Figures 2b and S1). Under 100% Fe growth conditions, both *wt* and βS188A *Av* cells displayed identical doubling times (3.9 h). Reducing the Fe concentration in the growth medium to 0.4 μM (hereafter referred to as 1% Fe) significantly slowed down the growth rates of both *Av* strains. However, βS188A cells experienced a more precipitous reduction in growth rate than *wt* cells with doubling times of 12.7 h and 6.3 h, respectively. The slower growth rate of *Av* βS188A cells relative to *wt* cells under Fe-limited growth conditions could potentially arise from differences in the expression levels of MoFeP and/or differences in the *in vivo* activity of βS188A and *wt* MoFeP.

To determine relative βS188A and *wt* MoFeP expression levels, we quantified MoFeP mRNA transcripts via quantitative reverse transcription PCR (RT-qPCR) of the *nifK* gene, which codes for the β-subunit of MoFeP. The values obtained were then normalized relative to the reference gene *rho*, a transcription termination factor that is constitutively expressed and has been used previously for *Av* RT-qPCR normalization (Figure 2c).[47] As a negative control, *nifK* transcript levels were measured under non-diazotrophic growth conditions, and not surprisingly, MoFeP expression was found to be downregulated for both *wt* and βS188A *Av* strains (Figure S2). We found that when grown diazotrophically under 100% Fe, βS188A and *wt Av* cells expressed MoFeP at the same level, suggesting that their identical growth rates resulted from both *wt* and βS188A *Av* MoFeP functioning with the same catalytic efficiency (Figure 2c). Thus, even if the βS188A P-cluster loses Fe during *in vivo* catalysis, reconstitution of the P-cluster is not rate-limiting under these conditions, which can be ascribed to the large LIP.

In contrast, *wt* and βS188A *Av* cells grown diazotrophically in the presence of 1% Fe exhibited *nifK* transcription levels that were 78% and 130% that of *wt* cells grown in 100% Fe media, respectively. The increase in βS188A's *nifK* expression taken together with the strain's slower growth rate under Fe-limiting conditions suggests that βS188A MoFeP does not function as efficiently as *wt* MoFeP under Fe-limited growth conditions. Thus, the cells are likely compensating via upregulation of MoFeP gene expression. This change in expression levels can be attributed to βS188A having slower P-cluster reconstitution at 1% Fe than at 100% Fe, and therefore, P-cluster reconstitution may become the rate-limiting step for N_2 fixation.

In vivo catalytic efficiencies of *wt* and βS188A MoFeP were probed by measuring whole cell acetylene (C_2H_2) reduction activity. The quantity of ethylene (C_2H_4) produced was normalized to the amount of MoFeP transcripts and the OD_{600} of the cells (Figure 2d). βS188A MoFeP from the 100% Fe culture and *wt* MoFeP from both 1% and 100% Fe cultures all had nearly identical cellular C_2H_2 reduction activities. In contrast, βS188A MoFeP in cells grown under 1% Fe displayed substantially reduced activity (<50% of *wt*), suggesting that βS188A MoFeP is not as catalytically efficient as the *wt* protein under limiting Fe conditions. Based on these results, we conclude that (1) βS188A MoFeP requires a larger LIP than *wt* MoFeP to operate efficiently under physiological conditions, and thus, (2) the P-cluster of βS188A MoFeP must be compositionally labile during catalysis under physiological conditions.

Dynamic, redox-dependent metal exchange by the βS188A P-cluster

Having determined the role of βS188 in maintaining the structural and functional integrity of the P-cluster under *in vivo* conditions, we investigated if the absence of this Ser ligand could also lead to dynamic metal exchange with the environment. We were interested in this possibility not only because it could furnish site-specifically metal-substituted variants of the P-cluster with unusual/useful electronic properties (as shown in the case of FeMoco),[48-49] but also because it could help demonstrate that a possible physiological role of βS188 may be to reduce the vulnerability of the P-cluster to mismetallation. We previously determined via X-ray crystallography that the two missing Fe centers in the oxidized βS188A P-cluster could be replenished upon reduction with DT to obtain the fully reconstituted the P-cluster.[19] This reconstitution did not require the addition of excess Fe, leading us to propose

that some of the MoFeP in solution could be "cannibalized" for its Fe content. This behavior is similar to the redox-labile [4Fe-4S] cluster of aconitase that can scavenge Fe from other protein-bound clusters upon re-reduction.[28, 50] Aconitase can also be reconstituted via the addition of excess reduced Fe to solution, minimizing the amount of protein clusters that are scavenged for Fe.[50]

We first investigated the ability of purified βS188A MoFeP to uptake Fe from solution (rather than from other MoFeP molecules) by reconstituting the oxidized P-cluster with $^{57}Fe^{2+}$, followed by the characterization of the isotopically labeled P-cluster by Mössbauer spectroscopy (Figure 3, green spectrum). The resulting spectrum is best fit by three quadrupole doublets (Table 1). Recording the spectrum at 54 mT clearly established that no FeMoco signals were present in the spectrum based on comparison to ^{57}Fe isotopically labeled FeMoco in *wt Av* MoFeP,[51] providing evidence that the incorporation of ^{57}Fe was specific to the P-clusters. McLean et al. termed the spectral components D (composed of D_1 and D_2), Fe^{2+}, and S, and determined that they accounted for 10, 4 and 2 Fe sites (4.2 K), respectively (Figure 3, black spectrum).[52] The D components in the spectrum are in close agreement with those observed for the ^{57}Fe-labeled P-clusters in MoFeP from *Klebsiella pneumoniae* (*Kp*),[52] indicating that ^{57}Fe was indeed incorporated into the P-clusters. Minor differences in isomer shifts and quadrupole splittings could arise from slight differences in the P-cluster environment in *Kp* and *Av.* Other *Kp* P-cluster doublets (S and Fe^{2+} sites) were not observed in the βS188A spectrum, however, as the parameters for D and S are quite similar, some contribution from the S component cannot be fully discounted. Regardless, our findings indicate that ^{57}Fe may not incorporate uniformly into every site in the P-cluster, or that the differences between the *Kp* and βS188A *Av* P-cluster environments may significantly shift the signals of some of the metal sites. We also observed an additional feature (Table 1, Figure 3, green spectrum, labeled as "adventitious $^{57}Fe^{2+}$") which closely matches the reported spectrum of aquated $^{57}FeSO_4$ and is consistent with adventitious $^{57}Fe^{2+}$ not associated with MoFeP.[53] To see if complete loss of the same ^{57}Fe-labeled Fe centers (presumably Fe1 and Fe5) occurred during each redox cycle, we performed a subsequent round of oxidation and reconstitution with the original Mössbauer sample, this time with natural-abundance Fe^{2+} (Figure 3, blue spectrum, Table S1). The peak intensities decreased significantly, but the features were not completely lost, demonstrating substantial but incomplete dissociation of ^{57}Fe from the βS188A P-clusters upon oxidation. The ratio of the peak areas in both spectra were nearly identical (Table S1). This observation may have two possible origins: incomplete loss of Fe from positions Fe1 and Fe5 during oxidation (Figure 1a) or shuffling of metals within the P-cluster during the reconstitution process.

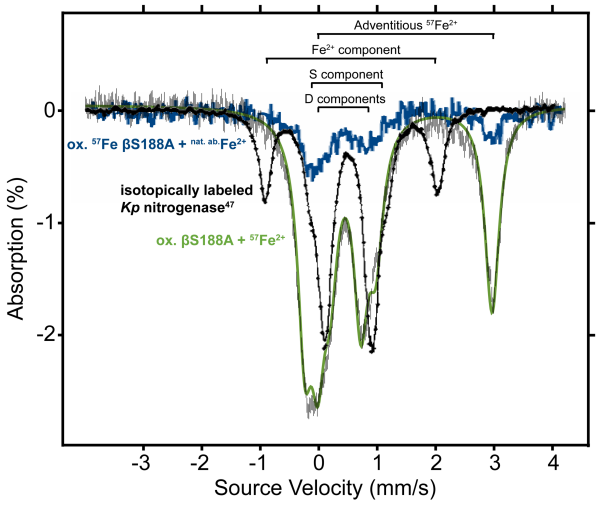

Figure 3. Mössbauer spectra of *Av* βS188A MoFeP reconstituted with ^{57}Fe-enriched or natural-abundance Fe in comparison to *Kp* MoFeP (previously reported). Spectra were recorded at 80 K and 54 mT. Oxidized βS188A was first reconstituted with $^{57}Fe^{2+}$ (green trace), followed by a second oxidation and reconstitution with natural abundance Fe^{2+} (blue trace). The spectrum of *Kp* MoFeP with ^{57}Fe-labelled P-clusters (black trace, 4.2 K, concentration unknown) is taken from reference 52 and is included as a comparison.

Table 1. Features observed in the Mössbauer spectrum of ^{57}Fe-reconstituted βS188A MoFeP.

Feature	ΔE_Q (mm/s)	δ (mm/s)	Relative area (%)
D_1	0.779	0.589	23.8
D_2	0.735	0.352	39.6
Adventitious $^{57}Fe^{2+}$	3.203	1.363	36.6

X-ray crystallographic analysis of heterometallated βS188A P-clusters

After establishing via Mössbauer spectroscopy that the βS188A P-cluster can be reconstituted with $^{57}Fe^{2+}$ from solution, we investigated if the cluster could be replaced with non-Fe metal ions (i.e., heterometals) upon oxidation *in vitro*. To this end, we determined the crystal structures of βS188A MoFeP reconstituted with Ga^{3+}, Ni^{2+}, and Co^{2+} (Figures 4, and S3, Table S2). To prepare these crystals, βS188A MoFeP was oxidized, reconstituted with the het-

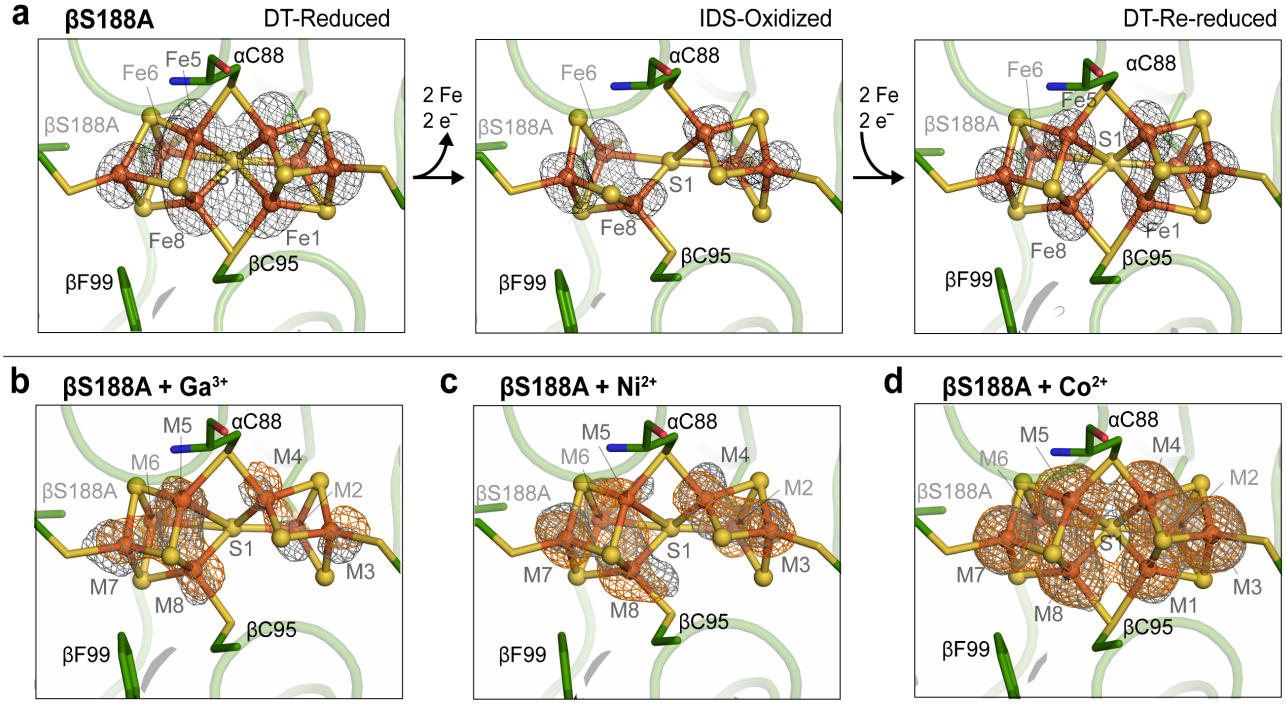

Figure 4. Crystal structures of *Av* βS188A MoFeP P-clusters. (a) Redox states of the βS188A P-clusters without heterometal: DT-reduced (left, PDB ID: 6O7L), IDS-oxidized (middle, PDB ID: 6O7S), and DT-re-reduced (right, PDB ID:6O7Q). Anomalous electron density difference maps depicting the location of the Fe-centers are in black mesh.[19] (b,c,d) Heterometallated βS188A P-clusters. Anomalous electron density difference maps (contoured at 4.5 σ) determined using X-ray diffraction data collected above and below the heterometal K-edge are shown in orange and gray mesh, respectively. Inorganic sulfides are depicted as yellow spheres and metals as orange spheres (modelled as Fe). (b) 2.2 Å structure of *Av* βS188A P-cluster reconstituted with Ga^{3+} contoured at 4.0 σ. (Above Ga K-edge: 10379 eV, Fe f" = 2.1, Ga f" = 3.9; below Ga K-edge: 10357 eV, Fe f" = 2.1, Ga f" = 0.5) (c) 2.0 Å structure of *Av* βS188A P-cluster reconstituted with Ni^{2+} contoured at 4.5 σ. (Above Ni K-edge: 8350 eV, Fe f" = 3.0, Ni f" = 3.9; below Ni K-edge: 8228 eV, Fe f" = 3.1, Ni f" = 0.5) (d) 2.0 Å structure of *Av* βS188A P-cluster reconstituted with Co^{2+} contoured at 4.5 σ. (Above Co K-edge: 7730 eV, Fe f" = 3.4, Co f" = 3.9; below Co K-edge: 7690 eV, Fe f" = 3.4, Co f" = 0.5)

erometal, and then crystallized in the presence of DT after removal of excess heterometal ions from the protein solution. We previously confirmed through X-ray crystallography[19] that the oxidized βS188A P-cluster could be fully reconstituted (i.e., 8.0 Fe atoms per P-cluster) upon crystallization in the presence of DT *without* addition of metal ions (Figure 4a). In contrast, the three heterometal-reconstituted βS188A MoFeP crystal structures crystallized in the presence of DT revealed P-clusters with a total metal occupancy of 5.7 to 7.4 metal atoms (integrated over the entire P-cluster) (Figure 4, Table 2). The occupied metal sites included positions that are normally vacant in the oxidized βS188A P-cluster (i.e., M1 and M5, where M refers to any metal ion), although the occupancy of these positions was not unity.

The incomplete occupancy of the metal sites in the presence of DT (unlike DT-re-reduced βS188A MoFeP without added metals) strongly suggests that the P-clusters are indeed heterometallated. Interestingly, the analysis of the metal-specific anomalous electron density maps determined both above and below the K-edge of the heterometal indicated that each metal-bound site displayed mixed occupancy for both Fe and the heterometal (Figure 4). Due to confounding factors such as the partial occupancy of heterometals and <1.0 total metal occupancy at each site, it was not possible to determine the absolute or relative occupancies of Fe or the heterometal at these positions. Therefore, in the databank-deposited structural models, we treated all occupied metal sites in the P-cluster as Fe-only. Total occupancy at each site was determined by refinement of metal at each site after refining B-factors, whereby B-factors were held constant at values relative to the inorganic sulfides.

We also examined the incorporation of heterometals into the P-cluster using inductively coupled plasma mass spectrometry (ICP-MS). The results, shown in Table S3, confirm that ^{57}Fe and heterometals can be incorporated into MoFeP only in the case of the βS188A variant but not *wt* MoFeP. We must also note that there were very large sample-dependent variations in the amounts of heterometals associated with MoFeP, which we interpret as further evidence for the highly dynamic nature of the oxidized βS188A P-cluster. We observed that the composition of the reconstituted βS188A P-cluster was dependent on the identity of the added heterometal. When the cluster was reconstituted with Ga^{3+} or Ni^{2+}, only seven of the eight P-cluster metal sites were populated by a metal ion (Figure 4b and 4c). On the other hand, incubation with Co^{2+} led to the occupation of all eight sites (Figure 4d). The higher efficiency of Co^{2+} to metallate the P-cluster may be attributed to its similarity to Fe^{2+} in terms of ionic radius and propensity to form tetrathiolate complexes with tetrahedral symmetry.[54]

Table 2. Crystallographic occupancies of each metal site in the re-reduced, heterometallated βS188A P-clusters

Metal site	DT-re-reduced βS188A	βS188A + Ga^{3+}	βS188A + Ni^{2+}	βS188A + Co^{2+}
M1	1.00	0.00	0.00	0.68
M2	1.00	0.87	0.74	0.92
M3	1.00	0.97	0.80	0.97
M4	1.00	0.89	0.74	1.00
M5	1.00	0.58	0.61	0.90
M6	1.00	0.98	0.99	0.94
M7	1.00	1.00	1.00	0.99
M8	1.00	0.95	0.83	0.96
Total	8.00	6.24	5.71	7.36

EPR analyses of heterometallated βS188A P-clusters

To further characterize the heterometallated P-clusters of βS188A, we collected electron paramagnetic resonance (EPR) spectra after reconstitution of the cluster with $^{57}Fe^{2+}$ and heterometals (Ga^{3+}, Ni^{2+}, and Co^{2+}) (Figure 5). βS188A and *wt* MoFeP were oxidized with indigo disulfonate (IDS) followed by the addition of $^{57}Fe^{2+}$ or the heterometals. Previously established $S = 3/2$ features ($g \approx 4.3$, 3.7, and 2.0) arising from FeMoco were present in all samples as expected.[55-57] Reconstitution of βS188A MoFeP with $^{57}Fe^{2+}$, Co^{2+}, and Ni^{2+} resulted in near identical features in the $g \approx 5$ region (Figure 5b) which were not detected in the *wt* samples (Figure 5a). Similar features have been observed in synthetic $NiFe_3S_4$ cubane clusters[58-59] and in *Pyrococcus furiosus* Fd that has been mismetallated with Cd[39] or Ni.[40] These observations are again consistent with the association of heterometals with the βS188A P cluster that does not occur in the *wt* MoFeP, in agreement with the crystallographic results (Figure 4). The possibility that heterometals may associate with FeMoco rather than the P-cluster was eliminated by the fact that the heterometal-treated *wt* MoFeP does not feature a $g \approx 5$ EPR signal (Figure 5a). The finding that the new

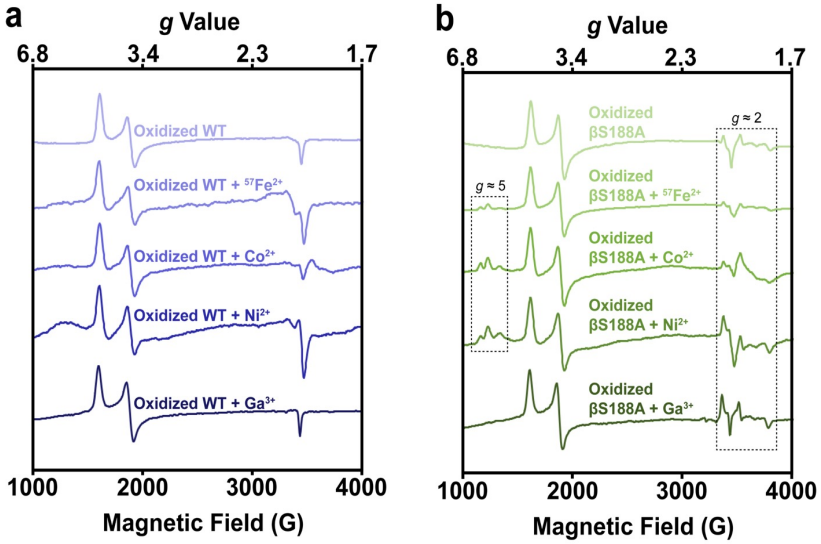

Figure 5. **X-band EPR spectra of *wt* and βS188A MoFeP after oxidation and soaking with heterometals collected at 4 K**. (a) IDS-oxidized wt *Av* MoFeP (top) soaked with $^{57}Fe^{2+}$, Co^{2+}, Ni^{2+}, and Ga^{3+} (top to bottom). (b) IDS-oxidized βS188A *Av* MoFeP (top) soaked with $^{57}Fe^{2+}$, Co^{2+}, Ni^{2+}, and Ga^{3+} (top to bottom). Reconstitution with $^{57}Fe^{2+}$, Co^{2+}, and Ni^{2+} resulted in new features in the $g \approx 5$ region. All metal-treated βS188A samples had features in the $g \approx 2$ region that closely resembled those for the oxidized βS188A species, but the features varied in intensity. Oxidized *wt* and βS188A spectra without added metals (top) are reproduced from reference 19 for comparison.

EPR features were similar in all cases of heterometallated βS188A MoFeP species–regardless of the identity of the heterometal–was unexpected. We tentatively ascribe this observation to an equal perturbation of the many close, low energy electronic states of the P-cluster[60] by heterometal substitution or changes in the population of a previously established $S = 5/2$ excited state of the cluster.[61] However, further in-depth spectroscopic studies will be required to identify the origin of these signals and understand their similarities among the various heterometals. Reconstitution of βS188A with Ga^{3+} did not produce the $g \approx 5$ signals, which may be rationalized by its frontier orbitals having much more p and less d character than the other heterometals used, resulting in substantially different electronic properties from the other heterometallic P-clusters. EPR spectra of all the reconstituted βS188A MoFeP species had additional features in the $g \approx 2$ region that closely resemble oxidized, metal-deficient βS188A MoFeP (Figure 5b),[19] and unusual P-cluster features seen in FeMoco-deficient MoFeP.[62] Of note, these features were weakest in the samples reconstituted with $^{57}Fe^{2+}$ and Co^{2+}, possibly due to the ability of these ions to occupy all eight P-cluster metal sites, creating a structurally more symmetrical and electronically more isotropic spin system.

As a control, EPR spectra were collected on both *wt* and βS188A MoFeP samples in which the IDS oxidation step was omitted (Figure S4). All *wt* spectra displayed only the expected FeMoco signals (Figure S4a). Ni^{2+}, Co^{2+}, and $^{57}Fe^{2+}$ were unable to incorporate into the reduced P-cluster as evidenced by the lack of features in the $g \approx 2$ and $g \approx 5$ regions (Figure S4b), confirming the full occupancy of all eight metal sites by iron in the P^N state. Unexpectedly, the Ga^{3+} treatment of the reduced βS188A MoFeP resulted in $g \approx 2$ features (Figure S4b), suggesting that Ga^{3+} may be capable of perturbing the electronic state of the βS188A P-cluster through an unidentified mechanism.

Conclusions

In this work, we have examined the potential role of a Ser ligand in maintaining the structural and functional integrity of the nitrogenase P-cluster under environmental duress. Our studies have demonstrated that (1) the growth of βS188A *Av* cultures is adversely affected by suboptimal growth conditions (i.e., Fe-limited growth media and oxidative stress) to a much greater extent than *wt Av* cells, (2) βS188A MoFeP has significantly lower *in vivo* catalytic activity than *wt* MoFeP, and (3) the oxidized [6Fe-7S] P-cluster of βS188A can be reconstituted with various exogenous metals ($^{57}Fe^{2+}$, Co^{2+}, Ni^{2+}, Ga^{3+}). Importantly, these heterometals are found to be distributed throughout the P-cluster rather than being localized to the positions of the displaced Fe centers. These findings highlight the role of the Ser ligand in protecting the P-cluster under stress conditions and demonstrate that this cluster is compositionally dynamic and readily capable of exchanging its atomic constituents. This attribute is shared by FeMoco, FeVco, and the [4Fe-4S] cluster of FeP which have also been shown to undergo substitution of their sulfur components under catalytically relevant conditions.[63-66]

Why has evolution selected a nearly invariant O-based ligand (Ser or Tyr) to the P-cluster when a similarly negatively charged and more common Cys could have potentially served the same role? We previously suggested that the hard, O-based Ser or Tyr side chains may be preferred over the soft, Cys thiolate due their strong preferences for binding Fe^{3+} over Fe^{2+}, allowing them to serve as redox-dependent switches that may be an integral component of the ET mechanism to the active site.[1, 18-20] This proposal is supported by fact that the *Av* βS188C MoFeP mutant is only ~60% as catalytically active as the *wt* protein for H^+ reduction,[11] and potentially even less active for the reduction of N_2. Our current results with βS188A MoFeP indicate that the role of the Ser ligand to the P-cluster may extend beyond acting merely as a redox switch and expand upon the known mechanisms that diazotrophic organisms have evolved to protect nitrogenase from oxidative stress.[67-70] It is reasonable to assume that a Tyr may fulfill an analogous functional role in nitrogenases lacking a Ser ligand to the P-cluster such as the previously characterized MoFeP from *Gd*.[18] Interestingly, there is only one known diazotrophic microbe that contains neither a Ser nor a Tyr P-cluster ligand, *Methanococcus aeolicus Nankai-3*.[18] This archaeon is a strict anaerobe that was isolated from marine sediments near the Nankai Trough,[71] an environment with unusually high Fe availability,[72] which may explain the ability of this organism to thrive without the protection of Ser or Tyr ligand to the P-cluster.

Materials and Methods

Reagents. All reagents were obtained from Fischer Scientific, Sigma-Aldrich, VWR International, Praxair, Roche Diagnostics, or New England Biolabs unless otherwise noted.

Growth media. All *Av* cultures were grown in Burke's medium (BM^+) containing 2.0% sucrose, 0.9 mM $CaCl_2$, 1.67 mM $MgSO_4$, 35 μM $FeSO_4$, 2 μM $Na_2Mo_2O_4$, 10 mM K_3PO_4 pH 7.5, and 10 mM NH_4Cl. Diazotrophic media

(BM^-) lacked NH_4Cl. Media with varying concentrations of iron are referred to as X% Fe, relative to 100% Fe (35 μM). Solid Burke's media contained 23 g/L agar. All growths were completed at 30°C and shaken at 200 rpm, unless otherwise noted. All OD_{600} values were measured using a cuvette with a 1 cm path length, unless otherwise noted.

Mutagenesis of *A. vinelandii* genome. The nitrogenase βS188A MoFeP mutant from a previous study was used in these experiments.[19].βS188A ΔnifB *Av* was generated by inserting a kanamycin resistance cassette into nifB using a plasmid (PDB218) kindly provided by V. Cash and D. Dean. This plasmid contained the cassette flanked by the beginning and end of the *nifB* gene. βS188A *Av* cells were made competent for transformation using an established procedure[73-74] by growing to OD_{600} = 0.5 in 50 mL 0% Fe BM^+ media, shaking at 150 rpm. As a result of Fe-starvation, cell cultures were fluorescent green due to excreted siderophores. 50 μL suspensions of competent cells were transformed in 50 μL transformation buffer solutions (20 mM MOPS, pH 7.5, 20 mM $MgSO_4$) containing 5 μg of PDB218. Transformation of *Av* cells using this protocol results in genomic modifications via double homologous recombination of the plasmid and the genome. Transformants were screened for kanamycin resistance on solid BM^+ media containing 5 μg/mL kanamycin (BM^+ Kan). Transformants were also streaked on solid BM^- to ensure that the N_2 fixation ability was lost. Multiple passes of the transformants on solid BM^+ Kan media were required for complete loss of N_2 fixation ability. The final transformant was verified with sequencing of the nifB region of the genome.

***A. vinelandii* culture growth**. *Av* cells were grown beginning with a 10- mL BM^- starter culture in a 500 mL Erlenmeyer flask until the cells reached a density of OD_{600} 1.5–2.0. 15 mL of the starter culture was used to inoculate 1.0 L of BM^- media in a 2.8-L flask (ΔnifB strains were grown in BM^+ Kan for all growth steps). Once the cells were densely grown (OD_{600} > 1.5), 400 mL of the culture was used to inoculate 50 L of BM^+ media with only 3 mM NH_4Cl in a 60-L fermenter (New Brunswick Scientific). Cells were monitored for derepression of nitrogenase (indicated by a spike in dissolved oxygen) and harvested 4 h later. Cells were concentrated to <6 L using a Pellicon 2 Tangential flow membrane (Eppendorf), then pelleted by centrifugation at 5000 rpm and 4°C. Wet cell pellets of ΔnifB strains were ~50 g, and cell pellets of *wt* and βS188A weighed >100 g. Cell pellets were stored at −80°C until cell lysis and protein purification.

Protein purification. All cell lysis and purification steps were performed anaerobically on a Schlenk line under ultra-high-purity Ar or in a Coy anaerobic chamber under 95% Ar/5% H_2 (<2 ppm O_2). All buffers and columns were prepared under anaerobic conditions. Cell pellets were thawed overnight at 4°C, then resuspended in a ~ 150 mL buffer solution, termed Eq (50 mM TRIS, pH 7.75, 200 mM NaCl, 5 mM DT, 0.1 mg/mL DNase I). The suspension was lysed at 16,000 psi N_2 using a microfluidizer (Microfluidics), and the lysate (dark brown) was centrifuged at 12,000 rpm for 75 min under anaerobic conditions. The resulting dark brown supernatant was loaded onto a DEAE Sepharose column (equilibrated with Eq) and washed overnight with 1.5 L of Eq. Nitrogenase component proteins were eluted using a linear NaCl gradient (200 to 500 mM NaCl at 2.5 mL/min for 1.0 L, 50 mM TRIS, pH 7.75, 5 mM DT). MoFeP and FeP eluted at conductivities of ~25 (~23 for the ΔnifB strains) and ~30 mS/cm, respectively. Fractions containing tge protein of interest were identified via denaturing sodium dodecyl sulfate polyacrylamide gel electrophoresis (SDS-PAGE). Fractions were then pooled and diluted 1.8-fold with a salt-free buffer solution (50 mM TRIS, pH 7.75, 0 mM NaCl, 5 mM DT). Proteins were independently concentrated on a DEAE column that was equilibrated with a salt-free buffer solution and rapidly eluted with a high-salt buffer solution (50 mM TRIS, pH 7.75, 500 mM NaCl, 5 mM DT). Proteins were further purified by gel filtration on a Sepharose 200 column (GE Healthcare), using a high-salt buffer solution (50 mM TRIS, pH 8.0, 500 mM NaCl, 5 mM DT). Pure protein containing fractions were identified via SDS-PAGE. The fractions were combined and concentrated to ~10 mg/mL with an Amicon concentrator (EMD/Millipore, ~20 psi 95% Ar/ 5% H_2, 30 kDa membrane for FeP, 100 kDa membrane for MoFeP). Concentrated proteins were stored in ~500 μL aliquots in cryovials in liquid N_2. Protein concentrations were determined using both Bradford assays and Fe-chelation assays (6.2 M guanidine-HCl, 2 mM 2,2-bipyridine, 10% glacial acetic acid) at 522 nm with an extinction coefficient of 8650 M^{-1} cm^{-1}.

Preparation of heterometallic- and ^{57}Fe-incorporated-P-cluster MoFeP. MoFeP was desalted over a 10-DG gravity flow column (Bio-Rad) that had been equilibrated with a buffer solution (50 mM TRIS, pH 8.0, 500 mM NaCl) to remove DT. The protein was concentrated to ~50 μM in 30 kDa Microcon centrifugal filters (EMD/Millipore) and then oxidized with 2.5 mM IDS for 1 h. The protein solution was run over another 10-DG gravity flow column that had been equilibrated with a buffer solution (50 mM TRIS, pH 8.0, 500 mM NaCl) to remove IDS. The protein was concentrated to ~50 μM in 30 kDa Microcon centrifugal filters (EMD/Millipore), followed by addition of 1 mM metal (M = $NiSO_4$, $CoCl_2$, $GaCl_3$, or $^{57}FeSO_4$). After a 1-h incubation, excess metal

was removed by exchanging the protein into a fresh buffer solution (50 mM TRIS, pH 8.0, 500 mM NaCl) with 30 kDa Microcon centrifugal filters (EMD/Millipore) and concentrated to ~50 μM. The first desalting and the IDS-oxidation steps were omitted during the preparation of the control EPR samples with reduced protein. All *wt* and βS188A MoFeP samples were prepared in parallel.

Mössbauer spectroscopy of MoFeP. The first Mössbauer sample was prepared as described above, followed by the concentration of the sample to 1 mM (400 μL final volume). After initial data collection, the sample was diluted to 125 μM. The sample was then re-metalated with natural abundance Fe^{2+} as described above, followed by the concentration of the sample back down to 1 mM. Mössbauer samples were prepared and flash frozen in liquid N_2 in a Coy anaerobic chamber under 95% Ar/5% H_2 (<2ppm O_2). Mössbauer spectra were recorded on a SEE Co. spectrometer in constant acceleration mode and transmission geometry at 80 K. A Janis SVT-300T dewar was used with a 54 mT magnetic field applied parallel to the propagation of the γ-beam. Isomer shifts were determined relative to the centroid of a metallic foil of a α-Fe at room temperature.

Crystallographic data collection and refinement. Crystals of heterometallated βS188A MoFeP were prepared using the sitting drop vapor diffusion method at room temperature under 95% Ar/5% H_2 (O_2 <2 ppm) in a Coy anaerobic chamber. All crystals were dark brown in color. Crystallization reservoirs each contained 500 μL of precipitation solution and crystallization wells contained 2 μL of the precipitation solution and 2 μL of the protein stock solution (125 μM). Crystals appeared within a few days and took up to two weeks to mature. Ni- and Co-substituted βS188A MoFeP crystals were grown from the same samples that were used in the EPR experiments. The crystal of the Ga-substituted variant was obtained using a sample prepared separately from the EPR samples. All proteins were crystallized in the presence of 10 mM DT. Crystals were cryoprotected with perfluoropolyether and flash frozen in liquid N_2 in a Coy anaerobic chamber. All data were collected using multi-wavelength synchrotron radiation at either SSRL beamline 9-2 (Ga- and Co-substituted structures) or ALS beamline 5.0.2 (Ni-substituted structure).

Data sets were integrated and scaled using iMosflm and Aimless, followed by molecular replacement (search model PDB 2MIN) with Phaser-MR of the PHENIX suite. Structures were refined with phenix.refine and Coot, using riding hydrogens added with phenix.reduce. Data collection and refinement parameters and statistics can be found in Table S2. All figures of crystal structures were produced with PyMOL. Integration with MAPMAN (Uppsala Software Factory) to assign partial occupancy of each metal (Fe and heterometal) at each metal site in the P-cluster was attempted.

Electron paramagnetic resonance spectroscopy of MoFeP. Samples were prepared as described in the "Preparation of heterometallic- and ^{57}Fe-incorporated-P-cluster MoFeP" sections above. Proteins were concentrated to 50 μM using 30 kDa Microcon centrifugal filters (EMD/Millipore). All data were collected on a Bruker EMX spectrometer. A helium cryostat was used to maintain temperatures in the range of 5−10K. The modulation frequency was 100.0 kHz and the modulation amplitude was 9.8 G during the recording of the spectra. The microwave frequency was ~9.62 GHz. Microwave power for each spectrum is indicated in figure captions. All spectra in figures were background subtracted.

MoFeP Fe-chelation assay. The Fe-chelation reactions contained 3.3 μM MoFeP, 13 mM DT, and 4.5 mM 2,2-bipyridine in a buffer solution (50 mM TRIS, pH 8.0, 500 mM NaCl) and were performed in an anaerobic cuvette (total reaction volume = 300 μL). The reaction was initiated by addition of the bipyridine at t = 0 min. Formation of the tris(bipyridine)iron(II) complex was monitored via absorbance at 520 nm over 15 min, and an extinction coefficient of 8650 M^{-1} cm^{-1} was used to calculate the concentration of the complex.

H_2O_2 oxidative stress survival test of *A. vinelandii*. *Av* cell cultures (*wt* and βS188A MoFeP) were grown in both BM^+ and BM^- media (200 rpm, 30°C) in biological triplicate until OD_{600} ~ 0.8. Dilutions of cells were plated on solid BM^+ or BM^- media (same as liquid growth conditions) to determine colony forming units (CFUs) present in the cultures prior to H_2O_2 exposure. Cultures were centrifuged (5,000 rpm, 4°C) to sediment the cells. The cell pellets were resuspended in fresh media (BM^+ and BM^- media corresponding to initial growth conditions) containing 5 mM Suprapur H_2O_2 (EMD Millipore) and shaken at 200 rpm and 30°C for 30 min. Cells were pelleted again via centrifugation (5,000 rpm, 4°C), then resuspended in fresh media (BM^+ and BM^- media corresponding to initial growth conditions) lacking H_2O_2. A dilution series of cells were plated to determine CFUs present after oxidative stress by H_2O_2. Colonies were manually counted 3-5 days after plating. The plates used for colony counting contained between 30-500 colonies.

Growth curves of *A. vinelandii*. All cultures used for growth curves were prepared in 125-mL flasks (pre-washed with nitric acid) containing 25 mL BM^- media (varying Fe %) and were shaken at 200 rpm, 30°C. *Wt* and βS188A

Av cells were initially Fe-starved by conducting four passes of the cells on solid 0% Fe BM^+ media, followed by one 25-mL liquid growth in 0% Fe BM^+ in a 125 mL flask until cells reached OD_{600} >1.0. Cells were fluorescent green due to secreted siderophores due to Fe starvation. Each variant (*wt* and βS188A MoFeP) of the Fe-starved cultures was used to inoculate five flasks of BM^- media with varying Fe concentrations (1%, 10%, 25%, 50%, and 100% Fe) to an initial OD_{600} of ~0.1. All media and culture growths were prepared in parallel. 200-μL aliquots were sterilely removed from each flask approximately every 4 h over the course of ~50 h to measure OD_{600}.

Extraction of total RNA from *Av* cells and RT-qPCR of MoFeP (*nifK*) transcripts. *Av* cells (*wt* and βS188A) were grown in biological triplicate to an OD_{600} of ~1.0 in 25 mL 100% and 1% Fe BM^- media with shaking at 200 rpm and 30 °C. 3 mL of cell suspensions were removed and added to 6 mL of RNAprotect Bacteria Reagent (Qiagen), immediately vortexed for 5 s and then incubated at room temperature for 5 min. Cells were centrifuged (5,000x g) for 10 min at room temperature, yielding a small, white pellet. The supernatant was removed, and pellets were frozen at −80 °C until RNA purification (total time frozen <1 week).

Total RNA purification was carried out using the RNeasy Mini Kit (Qiagen) using the prescribed protocols for enzymatic lysis of bacteria and purification of total RNA from bacterial lysate. Successful extraction of RNA was confirmed by visualizing rRNA bands with a 1% RNA agarose gel and quantified by UV-vis spectroscopy. Reverse transcription (RT) was carried out with Superscript III Reverse Transcriptase, random 9-mer primers, and 1 μg total RNA. cDNA products were confirmed via a smear on a 1% DNA agarose gel.

qPCR of the cDNA products was carried out using 10 ng of cDNA, Sybr dye, and Phusion HF polymerase in 20 μL total reaction volume in a Stratagene Mx3000 qPCR thermalcycler. qPCR reactions were carried out in technical triplicate of the biological replicates. Two housekeeping genes, *gyrA* and *rho*, were amplified as internal controls. However, *gyrA* provided inconsistent results. Data was thus normalized the *rho* reference gene. The following primers were used with an annealing temperature of 54 °C, resulting in an amplicons with a lengths of ~100 base pairs:

Forward *nifK* primer: CGAGACCTACCTGGGCAAC

Reverse *nifK* primer: CACTTCTTCCGGATCGGAGA

Forward *rho* primer: GGAAATGGCCGAACAGATGG

Reverse *rho* primer: GATTTCCTCGCCGCTTTTCG

Whole *A. vinelandii* cell C_2H_4 activity assays. Whole cell activity assays were performed with the same *Av* cell cultures that were used for total RNA extraction and RT-qPCR analysis. Immediately after removing a portion of cells for RNA extraction, 1.0 mL of whole cell suspensions was removed and placed in a 10-mL vial under air and sealed with a septum. 1.0 mL of C_2H_2 (room temperature, atmospheric pressure) was transferred into the headspace of the vial via gastight Hamilton syringe. Vials were shaken in a 30 °C water bath for 95 min. The product, C_2H_4, was quantified by gas chromatography (SRI 8610C) with an FID detector, using 0.2-mL injections of the headspace into a HayeSep N packed column (SRI Instruments). A standard curve of C_2H_4 was prepared daily with each experiment. *In vivo* relative specific activity of MoFeP was calculated using the relative quantities of *nifK* mRNA transcripts determined from RT-qPCR.

ORCID

Hannah L. Rutledge: 0000-0002-8672-2797
Mackenzie J. Field: 0000-0002-0935-2913
Jonathan Rittle: 0000-0001-6241-6253
Michael T. Green: 0000-0001-8658-8420.
F. Akif Tezcan: 0000-0002-4733-6500

Present Addresses

† J.R.: Department of Chemistry, University of California, Berkeley, Berkeley, California 94720, USA.

Author Contributions

The manuscript was written through contributions of all authors. All authors have given approval to the final version of the manuscript.

Notes

The authors declare no competing financial interests. Coordinate and structure factor files have been deposited into the RCSB databank under the following PDB IDs: 8E3T, 8E3U, 8E3V.

ACKNOWLEDGMENT

We thank C. Owens, J. Zhu, C.J. Yu, N. Avakyan, A. Kakkis, and R. Yu for critical discussions, V. Cash and D. Dean (Va. Tech) for generously providing the *Av* nifK knockout strain DJ200, and E. Lavorando for assistance with RT-qPCR experiments. This work was supported by the National Institutes of Health (Grant R01-GM099813) and by NASA (80NSSC18M0093; ENIGMA: Evolution of Nanomachines in Geospheres and Microbial Ancestors (NASA Astrobiology Institute Cycle 8)). H.L.R. was additionally supported by the Molecular Biophysics Training Grant (NIH Grant T32-GM008326).

REFERENCES

1. Rutledge, H. L.; Tezcan, F. A., Electron Transfer in Nitrogenase. *Chem. Rev.* **2020,** *120*, 5158-5193.
2. Seefeldt, L. C.; Yang, Z. Y.; Lukoyanov, D. A.; Harris, D. F.; Dean, D. R.; Raugei, S.; Hoffman, B. M., Reduction of Substrates by Nitrogenases. *Chem. Rev.* **2020,** *120*, 5082-5106.
3. Hoffman, B. M.; Lukoyanov, D.; Yang, Z. Y.; Dean, D. R.; Seefeldt, L. C., Mechanism of Nitrogen Fixation by Nitrogenase: The Next Stage. *Chem. Rev.* **2014,** *114*, 4041-4062.
4. Simpson, F. B.; Burris, R. H., A nitrogen pressure of 50 atmospheres does not prevent evolution of hydrogen by nitrogenase. *Science* **1984,** *224*, 1095-7.
5. Einsle, O.; Rees, D. C., Structural Enzymology of Nitrogenase Enzymes. *Chem. Rev.* **2020,** *120*, 4969-5004.
6. Howard, J. B.; Rees, D. C., Structural basis of biological nitrogen fixation. *Chem. Rev.* **1996,** *96*, 2965-2982.
7. Erickson, J. A.; Nyborg, A. C.; Johnson, J. L.; Truscott, S. M.; Gunn, A.; Nordmeyer, F. R.; Watt, G. D., Enhanced efficiency of ATP hydrolysis during nitrogenase catalysis utilizing reductants that form the all-ferrous redox state of the Fe protein. *Biochemistry* **1999,** *38*, 14279-85.
8. Lowery, T. J.; Wilson, P. E.; Zhang, B.; Bunker, J.; Harrison, R. G.; Nyborg, A. C.; Thiriot, D.; Watt, G. D., Flavodoxin hydroquinone reduces *Azotobacter vinelandii* Fe protein to the all-ferrous redox state with a S = 0 spin state. *Proc. Natl. Acad. Sci. U. S. A.* **2006,** *103*, 17131-6.
9. Hardy, R. W. F.; Knight, E., Reductant-Dependent Adenosine Triphosphatase of Nitrogen-Fixing Extracts of *Azotobacter vinelandii*. *Biochim. Biophys. Acta* **1966,** *122*, 520-&.
10. Chan, J. M.; Christiansen, J.; Dean, D. R.; Seefeldt, L. C., Spectroscopic evidence for changes in the redox state of the nitrogenase P-cluster during turnover. *Biochemistry* **1999,** *38*, 5779-5785.
11. Danyal, K.; Dean, D. R.; Hoffman, B. M.; Seefeldt, L. C., Electron Transfer within Nitrogenase: Evidence for a Deficit-Spending Mechanism. *Biochemistry* **2011,** *50*, 9255-9263.
12. Johnson, D. C.; Dean, D. R.; Smith, A. D.; Johnson, M. K., Structure, function, and formation of biological iron-sulfur clusters. *Annu. Rev. Biochem.* **2005,** *74*, 247-81.
13. Cammack, R., Iron-Sulfur Clusters in Enzymes - Themes and Variations. *Adv. Inorg. Chem.* **1992,** *38*, 281-322.
14. Liu, J.; Chakraborty, S.; Hosseinzadeh, P.; Yu, Y.; Tian, S.; Petrik, I.; Bhagi, A.; Lu, Y., Metalloproteins containing cytochrome, iron-sulfur, or copper redox centers. *Chem. Rev.* **2014,** *114*, 4366-469.
15. Peters, J. W.; Stowell, M. H.; Soltis, S. M.; Finnegan, M. G.; Johnson, M. K.; Rees, D. C., Redox-dependent structural changes in the nitrogenase P-cluster. *Biochemistry* **1997,** *36*, 1181-7.
16. Cao, L.; Borner, M. C.; Bergmann, J.; Caldararu, O.; Ryde, U., Geometry and Electronic Structure of the P-Cluster in Nitrogenase Studied by Combined Quantum Mechanical and Molecular Mechanical Calculations and Quantum Refinement. *Inorg. Chem.* **2019**.
17. Keable, S. M.; Zadvornyy, O. A.; Johnson, L. E.; Ginovska, B.; Rasmussen, A. J.; Danyal, K.; Eilers, B. J.; Prussia, G. A.; LeVan, A. X.; Raugei, S.; Seefeldt, L. C.; Peters, J. W., Structural characterization of the P^{1+} intermediate state of the P-cluster of nitrogenase. *J. Biol. Chem.* **2018,** *293*, 9629-9635.
18. Owens, C. P.; Katz, F. E.; Carter, C. H.; Oswald, V. F.; Tezcan, F. A., Tyrosine-Coordinated P-Cluster in *G. diazotrophicus* Nitrogenase: Evidence for the Importance of O-Based Ligands in Conformationally Gated Electron Transfer. *J. Am. Chem. Soc.* **2016,** *138*, 10124-7.
19. Rutledge, H. L.; Rittle, J.; Williamson, L. M.; Xu, W. A.; Gagnon, D. M.; Tezcan, F. A., Redox-Dependent Metastability of the Nitrogenase P-Cluster. *J. Am. Chem. Soc.* **2019,** *141*, 10091-10098.

20. Seefeldt, L. C.; Hoffman, B. M.; Peters, J. W.; Raugei, S.; Beratan, D. N.; Antony, E.; Dean, D. R., Energy Transduction in Nitrogenase. *Acc. Chem. Res.* **2018,** *51*, 2179-2186.
21. Rutledge, H. L.; Cook, B. D.; Nguyen, H. P. M.; Herzik, M. A., Jr.; Tezcan, F. A., Structures of the nitrogenase complex prepared under catalytic turnover conditions. *Science* **2022,** *377*, 865-869.
22. Berkovitch, F.; Nicolet, Y.; Wan, J. T.; Jarrett, J. T.; Drennan, C. L., Crystal structure of biotin synthase, an S-adenosylmethionine-dependent radical enzyme. *Science* **2004,** *303*, 76-79.
23. McLaughlin, M. I.; Lanz, N. D.; Goldman, P. J.; Lee, K. H.; Booker, S. J.; Drennan, C. L., Crystallographic snapshots of sulfur insertion by lipoyl synthase. *Proc. Natl. Acad. Sci. U. S. A.* **2016,** *113*, 9446-9450.
24. Nicolet, Y.; Rohac, R.; Martin, L.; Fontecilla-Camps, J. C., X-ray snapshots of possible intermediates in the time course of synthesis and degradation of protein-bound Fe_4S_4 clusters. *Proc. Natl. Acad. Sci. U. S. A.* **2013,** *110*, 7188-92.
25. Holm, R. H., Trinuclear Cuboidal and Heterometallic Cubane-Type Iron-Sulfur Clusters - New Structural and Reactivity Themes in Chemistry and Biology. *Adv. Inorg. Chem.* **1992,** *38*, 1-71.
26. Brown, O. R.; Smyk-Randall, E.; Draczynska-Lusiak, B.; Fee, J. A., Dihydroxy-acid dehydratase, a [4Fe-4S] cluster-containing enzyme in Escherichia coli: effects of intracellular superoxide dismutase on its inactivation by oxidant stress. *Arch. Biochem. Biophys.* **1995,** *319*, 10-22.
27. Flint, D. H.; Emptage, M. H.; Guest, J. R., Fumarase-a from Escherichia-Coli - Purification and Characterization as an Iron Sulfur Cluster Containing Enzyme. *Biochemistry* **1992,** *31*, 10331-10337.
28. Beinert, H.; Kennedy, M. C.; Stout, C. D., Aconitase as iron-sulfur protein, enzyme, and iron-regulatory protein. *Chem. Rev.* **1996,** *96*, 2335-2373.
29. Robbins, A. H.; Stout, C. D., Structure of Activated Aconitase - Formation of the [4Fe-4S] Cluster in the Crystal. *Proc. Natl. Acad. Sci. U. S. A.* **1989,** *86*, 3639-3643.
30. Lauble, H.; Kennedy, M. C.; Beinert, H.; Stout, C. D., Crystal structures of aconitase with isocitrate and nitroisocitrate bound. *Biochemistry* **1992,** *31*, 2735-48.
31. Flint, D. H.; Tuminello, J. F.; Emptage, M. H., The Inactivation of Fe-S Cluster Containing Hydro-Lyases by Superoxide. *J. Biol. Chem.* **1993,** *268*, 22369-22376.
32. Imlay, J. A., Iron-sulphur clusters and the problem with oxygen. *Mol. Microbiol.* **2006,** *59*, 1073-1082.
33. Imlay, J. A., Cellular defenses against superoxide and hydrogen peroxide. *Annu. Rev. Biochem.* **2008,** *77*, 755-76.
34. Imlay, J. A., The molecular mechanisms and physiological consequences of oxidative stress: lessons from a model bacterium. *Nat. Rev. Microbiol.* **2013,** *11*, 443-454.
35. Kuo, C. F.; Mashino, T.; Fridovich, I., Alpha,Beta-Dihydroxyisovalerate Dehydratase - a Superoxide-Sensitive Enzyme. *J. Biol. Chem.* **1987,** *262*, 4724-4727.
36. Varghese, S.; Tang, Y.; Imlay, J. A., Contrasting sensitivities of Escherichia coli aconitases A and B to oxidation and iron depletion. *J. Bacteriol.* **2003,** *185*, 221-230.
37. Martic, M.; Jakab-Simon, I. N.; Haahr, L. T.; Hagen, W. R.; Christensen, H. E. M., Heterometallic $[AgFe_3S_4]$ ferredoxin variants: synthesis, characterization, and the first crystal structure of an engineered heterometallic iron-sulfur protein. *J. Biol. Inorg. Chem.* **2013,** *18*, 261-276.
38. Finnegan, M. G.; Conover, R. C.; Park, J. B.; Zhou, Z. H.; Adams, M. W. W.; Johnson, M. K., Electronic, Magnetic, Redox, and Ligand-Binding Properties of [MFe(3)S(4)] Clusters (M=Zn, CO, Mn) in Pyrococcus-Furiosus Ferredoxin. *Inorg. Chem.* **1995,** *34*, 5358-5369.
39. Staples, C. R.; Dhawan, I. K.; Finnegan, M. G.; Dwinell, D. A.; Zhou, Z. H.; Huang, H. S.; Verhagen, M. F. J. M.; Adams, M. W. W.; Johnson, M. K., Electronic, magnetic, and redox properties of [MFe3S4] clusters (M = Cd, Cu, Cr) in Pyrococcus furiosus ferredoxin. *Inorg. Chem.* **1997,** *36*, 5740-5749.
40. Conover, R. C.; Park, J. B.; Adams, M. W. W.; Johnson, M. K., Formation and Properties of a Nife3s4 Cluster in Pyrococcus-Furiosus Ferredoxin. *J. Am. Chem. Soc.* **1990,** *112*, 4562-4564.
41. Fu, W. G.; Telser, J.; Hoffman, B. M.; Smith, E. T.; Adams, M. W. W.; Finnegan, M. G.; Conover, R. C.; Johnson, M. K., Interaction of Tl+ and Cs+ with the [Fe3s4] Cluster of Pyrococcus-Furiosus Ferredoxin - Investigation by Resonance Raman, MCD, EPR, and Endor Spectroscopy. *J. Am. Chem. Soc.* **1994,** *116*, 5722-5729.
42. Faridoon, K. Y.; Zhuang, H. Y.; Sykes, A. G., Kinetic Studies on the Reaction of M^{2+} Ions with Aconitase Fe3S40 To Give $Fe_3MS_4^{2+}$ Clusters (M = Fe, Mn, Co). *Inorg. Chem.* **1994,** *33*, 2209-2212.
43. Sandercock, J. R.; Page, W. J., RpoS expression and the general stress response in Azotobacter vinelandii during carbon and nitrogen diauxic shifts. *J. Bacteriol.* **2008,** *190*, 946-53.

44. Rodriguez-Rojas, A.; Kim, J. J.; Johnston, P. R.; Makarova, O.; Eravci, M.; Weise, C.; Hengge, R.; Rolff, J., Non-lethal exposure to H_2O_2 boosts bacterial survival and evolvability against oxidative stress. *PLoS Genet.* **2020,** *16*.

45. Orikasa, Y.; Nodasaka, Y.; Ohyama, T.; Okuyama, H.; Ichise, N.; Yumoto, I.; Morita, N.; Wei, M.; Ohwada, T., Enhancement of the nitrogen fixation efficiency of genetically-engineered Rhizobium with high catalase activity. *J. Biosci. Bioeng.* **2010,** *110*, 397-402.

46. Page, W. J.; Huyer, M., Derepression of the Azotobacter-Vinelandii Siderophore System, Using Iron-Containing Minerals to Limit Iron Repletion. *J. Bacteriol.* **1984,** *158*, 496-502.

47. Noguez, R.; Segura, D.; Moreno, S.; Hernandez, A.; Juarez, K.; Espin, G., Enzyme I NPr, NPr and IIA Ntr are involved in regulation of the poly-beta-hydroxybutyrate biosynthetic genes in Azotobacter vinelandii. *J. Mol. Microbiol. Biotechnol.* **2008,** *15*, 244-54.

48. Srisantitham, S.; Badding, E. D.; Suess, D. L. M., Postbiosynthetic modification of a precursor to the nitrogenase iron-molybdenum cofactor. *Proc. Natl. Acad. Sci. U. S. A.* **2021,** *118*, e2015361118.

49. Badding, E.; Srisantitham, S.; Lukoyanov, D.; Hoffman, B. M.; Suess, D., Connecting the Geometric and Electronic Structures of the Nitrogenase Iron–Molybdenum Cofactor through Site-Selective Labeling. *ChemRxiv* **2022**. doi: 10.26434/chemrxiv-2022-m57j9

50. Kennedy, M. C.; Emptage, M. H.; Dreyer, J. L.; Beinert, H., The role of iron in the activation-inactivation of aconitase. *J. Biol. Chem.* **1983,** *258*, 11098-105.

51. Yoo, S. J.; Angove, H. C.; Papaefthymiou, V.; Burgess, B. K.; Münck, E., Mössbauer Study of the MoFe Protein of Nitrogenase from Azotobacter vinelandii Using Selective 57Fe Enrichment of the M-Centers. *J. Am. Chem. Soc.* **2000,** *122*, 4926-4936.

52. McLean, P. A.; Papaefthymiou, V.; Orme-Johnson, W. H.; Münck, E., Isotopic hybrids of nitrogenase. Mossbauer study of MoFe protein with selective ^{57}Fe enrichment of the P-cluster. *J. Biol. Chem.* **1987,** *262*, 12900-3.

53. Rittle, J.; Field, M. J.; Green, M. T.; Tezcan, F. A., An efficient, step-economical strategy for the design of functional metalloproteins. *Nat. Chem.* **2019,** *11*, 434-441.

54. Vasak, M.; Kagi, J. H., Metal thiolate clusters in cobalt(II)-metallothionein. *Proc. Natl. Acad. Sci. U. S. A.* **1981,** *78*, 6709-13.

55. Van Stappen, C.; Decamps, L.; Cutsail, G. E.; Bjornsson, R.; Henthorn, J. T.; Birrell, J. A.; DeBeer, S., The Spectroscopy of Nitrogenases. *Chem. Rev.* **2020,** *120*, 5005-5081.

56. Munck, E.; Rhodes, H.; Orme-Johnson, W. H.; Davis, L. C.; Brill, W. J.; Shah, V. K., Nitrogenase. VIII. Mossbauer and EPR spectroscopy. The MoFe protein component from *Azotobacter vinelandii* OP. *Biochim. Biophys. Acta* **1975,** *400*, 32-53.

57. Rawlings, J.; Shah, V. K.; Chisnell, J. R.; Brill, W. J.; Zimmermann, R.; Münck, E.; Orme-Johnson, W. H., Novel metal cluster in the iron-molybdenum cofactor of nitrogenase. Spectroscopic evidence. *J. Biol. Chem.* **1978,** *253*, 1001-4.

58. Ciurli, S.; Ross, P. K.; Scott, M. J.; Yu, S. B.; Holm, R. H., Synthetic Nickel-Containing Heterometal Cubane-Type Clusters with Nife3q4 Cores (Q = S, Se). *J. Am. Chem. Soc.* **1992,** *114*, 5415-5423.

59. Zhou, J.; Scott, M. J.; Hu, Z. G.; Peng, G.; Munck, E.; Holm, R. H., Synthesis and Comparative Reactivity and Electronic Structural Features of $[MFe_3S_4]Z+$ Cubane-Type Clusters (M = Fe, CO, Ni). *J. Am. Chem. Soc.* **1992,** *114*, 10843-10854.

60. Li, Z.; Guo, S.; Sun, Q.; Chan, G. K., Electronic landscape of the P-cluster of nitrogenase as revealed through many-electron quantum wavefunction simulations. *Nat. Chem.* **2019**.

61. Tittsworth, R. C.; Hales, B. J., Detection of EPR Signals Assigned to the 1-Equiv-Oxidized P-Clusters of the Nitrogenase MoFe-Protein from *Azotobacter vinelandii*. *J. Am. Chem. Soc.* **1993,** *115*, 9763-9767.

62. Ribbe, M. W.; Hu, Y.; Guo, M.; Schmid, B.; Burgess, B. K., The FeMoco-deficient MoFe protein produced by a nifH deletion strain of Azotobacter vinelandii shows unusual P-cluster features. *J. Biol. Chem.* **2002,** *277*, 23469-76.

63. Spatzal, T.; Perez, K. A.; Howard, J. B.; Rees, D. C., Catalysis-dependent selenium incorporation and migration in the nitrogenase active site iron-molybdenum cofactor. *Elife* **2015,** *4*, e11620.

64. Kang, W.; Lee, C. C.; Jasniewski, A. J.; Ribbe, M. W.; Hu, Y., Structural evidence for a dynamic metallocofactor during N2 reduction by Mo-nitrogenase. *Science* **2020,** *368*, 1381-1385.

65. Sippel, D.; Rohde, M.; Netzer, J.; Trncik, C.; Gies, J.; Grunau, K.; Djurdjevic, I.; Decamps, L.; Andrade, S. L. A.; Einsle, O., A bound reaction intermediate sheds light on the mechanism of nitrogenase. *Science* **2018,** *359*, 1484-1489.

66. Buscagan, T. M.; Kaiser, J. T.; Rees, D. C., Selenocyanate derived Se-incorporation into the Nitrogenase Fe protein cluster. *Elife* **2022,** *11*.

67. Schlesier, J.; Rohde, M.; Gerhardt, S.; Einsle, O., A Conformational Switch Triggers Nitrogenase Protection from Oxygen Damage by Shethna Protein II (FeSII). *J. Am. Chem. Soc.* **2016,** *138*, 239-47.

68. Medina, M. S.; Bretzing, K. O.; Aviles, R. A.; Chong, K.; Espinoza, A.; Garcia, C. N. G.; Katz, B. B.; Kharwa, R. N.; Hernandez, A.; Lee, J. L.; Lee, T. M.; Strul, M. W.; Lo Verde, C.; Wong, E. Y.; Owens, C. P., CowN sustains nitrogenase turnover in the presence of the inhibitor carbon monoxide. *J. Biol. Chem.* **2021**, 100501.

69. Mus, F.; Colman, D. R.; Peters, J. W.; Boyd, E. S., Geobiological feedbacks, oxygen, and the evolution of nitrogenase. *Free Radical Biol. Med.* **2019,** *140*, 250-259.

70. Varghese, F.; Kabasakal, B. V.; Cotton, C. A. R.; Schumacher, J.; Rutherford, A. W.; Fantuzzi, A.; Murray, J. W., A low-potential terminal oxidase associated with the iron-only nitrogenase from the nitrogen-fixing bacterium Azotobacter vinelandii. *J. Biol. Chem.* **2019,** *294*, 9367-9376.

71. Kendall, M. M.; Liu, Y.; Sieprawska-Lupa, M.; Stetter, K. O.; Whitman, W. B.; Boone, D. R., Methanococcus aeolicus sp. nov., a mesophilic, methanogenic archaeon from shallow and deep marine sediments. *Int. J. Syst. Evol. Microbiol.* **2006,** *56*, 1525-1529.

72. Torres, M. E.; Cox, T.; Hong, W.-L.; McManus, J.; Sample, J. C.; Destrigneville, C.; Gan, H. M.; Gan, H. Y.; Moreau, J. W., Crustal fluid and ash alteration impacts on the biosphere of Shikoku Basin sediments, Nankai Trough, Japan. *Geobiology* **2015,** *13*, 562-580.

73. Glick, B. R.; Brooks, H. E.; Pasternak, J. J., Transformation of *Azotobacter vinelandii* with plasmid DNA. *J. Bacteriol.* **1985,** *162*, 276-9.

74. Page, W. J.; Von Tigerstrom, M., Optimal Conditions for Transformation of *Azotobacter vinelandii*. *J. Bacteriol.* **1979,** *139*, 1058-1061.